ELSEVIER

Biochimica et Biophysica Acta 1325 (1997) 165–177

BIOCHIMICA ET BIOPHYSICA ACTA
BBA

Time-resolved X-ray reflectivity measurements of protein binding onto model lipid membranes at the air–water interface

Ulrich Vierl, Gregor Cevc

Medizinische Biophysik, Technische Universität München, Klinikum r.d.I., Ismaningerstr. 22, D-81675 München, Germany

Received 3 May 1996; accepted 5 December 1996

Abstract

The energy-dispersive X-ray reflectometry and turbidity measurements are used to investigate the kinetics of concanavalin A binding onto the distearoylphosphatidylcholine/distearoylphosphatidylethanolamine-maltobionamide (DSPC/DSPE-mal$_1$) or distearoylphosphatidylcholine/distearoylphosphatidylethanolamine-maltotetrabionamide (DSPC/mal$_3$) mixed monolayer at the air-water interface. The resulting adsorbed layer of this sugar-binding protein near the membrane with one or three hexoses in the lipid head-group is 3.9 nm or 9.7 nm thick, respectively. The different thicknesses of the adsorbed layer can be correlated with the diverse orientations of the adsorbed proteins. These lay flat on the surface containing DSPE-mal$_1$ and 'perpendicular' to the surface containing DSPE-mal$_3$. The monolayer structure is little affected by concanavalin A binding, but the incorporation of sugar lipids decreases the chain tilt and the interfacial thickness marginally. The binding is quasi-exponential with the time constant between some minutes and several hours depending on the concanavalin A and vesicle concentrations in the bulk. The experimental resolution of the time-resolved measurements made with the laboratory-based instrument is 15 min and the spatial resolution is between 0.05 nm and 0.5 nm, depending on the electron contrast. It is estimated that the high-brilliance synchrotron X-ray source combined with the detection method outlined in this work, could permit the kinetic measurements on the time-scale of < 1 minute.

PACS: 6810; 8715; 8720

Keywords: Glycolipid; Concanavalin A; Phosphatidylcholine; Molecular recognition; Structural investigation; Kinetics

1. Introduction

The technique of X-ray and neutron reflectivity is now well established for the investigations of solid and liquid surfaces as well as for the studies of corresponding surface layers (for an overview see [13]). Initially, all X-ray reflectometric measurements relied on the use of synchrotron radiation. In the last years it became clear, however, that good reflectivity experiments are also possible with the rotating anode or with the sealed X-ray tubes [9]. This has permitted in-house experimentation but the disadvantage of such low intensity X-ray sources to date were the very long exposure-times, which have precluded the fast or kinetic reflectometric measurements.

We have recently introduced the energy-dispersive reflectivity measurements into the field of fluid surface studies [16]. This allowed us to reduce the

PII S0005-2736(96)00253-2

data-recording time by the factor of 10 at least and has also made experiments on the time-scale of less than one hour possible.

Here we show that such rapid data acquisition is suitable for kinetic measurements on the time scale of minutes with a spatial resolution of approx. 0.3 nm. We illustrate this by investigating the binding of proteins onto the mixed lipid monolayer at the air–water interface with a laboratory based equipment designed for the energy-dispersive reflectometry detection. Sugar-binding protein concanavalin A is used as an example, owing to its significance in the biochemical research.

2. Materials and methods

1,2-Distearoyl-*sn*-glycero-3-phosphocholine (DSPC, purity $> 99\%$) was purchased from Boehringer-Mannheim (Germany, EU) and concanavalin A (concanavalin A, purity $> 99\%$) was from Sigma (Munich, Germany, EU). 1,2-Distearoyl-*sn*-glycero-3-ethanolamine-maltobionamide (DSPE-mal$_1$) and 1,2-distearoyl-*sn*-glycero-3-ethanolamine-maltotetrabionamide (DSPE-mal$_3$) was synthesized and purified in this laboratory as described before [3], according to the method of Williams et al. [18]. The purity of lipids was controlled by the thin-layer chromatography on silicic acid plates using $CHCl_3/MeOH/NH_2OH$ (65/15/3 V) as eluent and sulfuric acid staining followed by charring at 300 degrees for the detection. Water (18 MΩ/cm) was doubly distilled and reprocessed by a water purification unit (model Elgastat UHQ, ELGA Ltd., UK). Lipid-mixtures were spread from a chloroform solution (1 mg/ml) to create a monolayer at the air–water interface with the packing parameters corresponding to those of DSPC bilayers in the ordered-lamellar (L'_β) phase. The very different solubility of DSPC and DSPE-mal$_1$ and DSPE-mal$_3$ could lead to the monolayer-composition changes with time, owing to the material loss into the bulk. We have prevented this by keeping the corresponding suspension of lipid vesicles (extruded, diameter ≈ 200 nm, 10 mg/ml (for the DSPE-mal$_1$ measurements) or sonicated, diameter ≈ 70 nm, 0.3 mg/ml (for the DSPE-mal$_3$ measurements)) in the bulk. The lipid vesicles composition was identical to that of the surface-attached lipid monolayer; this maintained the lipid vesicles and lipid monolayer in equilibrium during the whole experiment.

Prior to the first X-ray measurement the lipid monolayer at the air–water interface was equilibrated at room-temperature for 5 h. Concanavalin A was then dissolved in 10 mM sodium chloride solution at the concentration of 1 mg/ml at pH of pure water and injected into the bulk under the monolayer to yield the final, desired protein concentration as given in the text.

2.1. X-ray reflectometry

Measurements were done on two different instruments. Both were based on a simple X-ray generator (Seifert, Ahrensburg, Germany, or Philips, Kassel, Germany) and equipped with a 3 kW (Mo) or 2 kW (W) sealed tube. Solid state detectors (Silena, Hasselroth, Germany, EU) with a high purity Ge-crystal and an excellent energy resolution of about 1% were used as energy analyzer. This permitted the angle- as well as energy-dispersive reflectivity measurements. The angles of incident and reflected beams, in the first reflectometer, were adjusted by vertically positioning the sample, the entrance slit, and the detector [12]. In the second reflectometer, the inclination of the tube- and detector holders as well as the vertical position of the sample chamber and of the detector holder were used for the same purpose (Fig. 1). X-ray beam in this latter case was collimated by two cross-slits minimizing the beam divergence. This improved the resolution and signal-to-noise ratio considerably.

2.2. Bulk measurements

To monitor protein binding to the lipid vesicles in the bulk, the turbidity of a suspension of sonicated vesicles was detected at 325 nm in a UV/vis spectrometer (Beckman spectrophotometer, Model 24, USA) under constant temperature conditions and stirring.

2.3. Theoretical background

2.3.1. Energy dispersive measurement of X-ray reflectivity

The intensity of the specularly reflected beam, as recorded in an energy-dispersive measurement, is

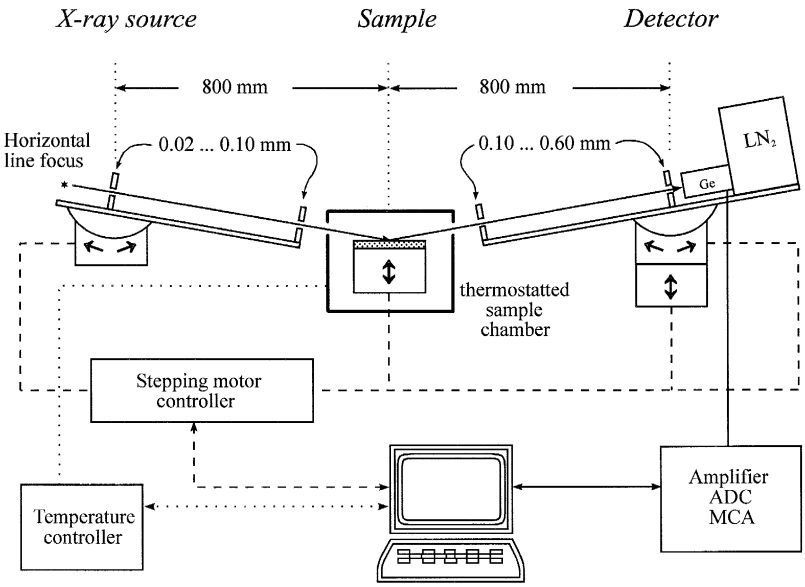

Fig. 1. Schematic side view of the reflectometer used for most of the studies described in this work. Horizontal slit widths were chosen to be 4.00 mm.

related to surface reflectivity, R, by the following equation [16]:

$$I(E) = R(q_z) \cdot g(E) \quad (1)$$

Function $g(E)$ is given by the product of an unknown energy distribution function in the spectrum of X-ray tube, the detector sensitivity, and a function which allows for all secondary energy-dependent effects, such as the scattering on the air and water vapor. The vertical wave vector transfer, q_z, is a function of the X-ray energy and incident angle θ.

In order to determine the function $g(E)$, we have first measured the reflectivity of a pure water surface in the angle-dispersive mode. The energy spectrum of the corresponding specularly reflected intensity, $I(E)$, was then recorded at all angles used in the energy-dispersive measurements. The calibration function $g(E)$ was deduced by means of Eq. (1), after background subtraction. Details of this procedure are given elsewhere [16].

2.3.2. X-ray reflectivity

Electron density profile perpendicular to the surface was calculated from the reflectivity curve by using the following 'master equation' in combination with a Gaussian-smeared box-model [11]:

$$R(q_z) = R_F(q_z) \cdot \left| \int \frac{\partial \rho(z)}{\partial z} e^{2iq_z z} dz \right|^2 \quad (2)$$

where $\rho(z)$ is the laterally averaged relative electron density: $\rho(z) = \rho_e(z)/\rho_e(z \rightarrow \ )$. The reflectivity of the Gaussian-smeared box-model, $R(q_z)/R_F(q_z)$, can be factorized in one factor depending only on the box heights and thicknesses and one factor that depends on the global interfacial roughness σ merely and has the form of a Debye-Waller factor:

$$\frac{R(q_z)}{R_F(q_z)} = R_{box}(q_z) \cdot e^{-q_z^2 \sigma^2} \quad (3)$$

By minimizing the difference between the calculated and the measured reflectivity curves by standard methods (Levenberg-Marquardt algorithm or combined Monte-Carlo/simulated annealing method), a model profile is derived from the experimental data.

2.3.3. Model for calculating the electron density profile

The measured reflectivity changes suggest that proteins from the solution adsorb (bind) to the lipid (mono)layer. To calculate the reflectivity of the resulting inhomogeneous surface, it is necessary to superimpose the scattering contributions of two different domains corresponding to the covered and uncovered monolayer. Such a superposition can be performed in two different ways [11]. If the scale of

the lateral film inhomogeneity is smaller than the lateral coherence length of the X-radiation ($\lesssim$ of the order of a few μm [14]), the electron density of both kind of domains must be averaged, that is, weighted by the covering efficiency, before inserting the resulting mean density profile into Eq. (2). This is so-called coherent superposition. If the typical dimensions of the different surface domains are larger than the lateral coherence length of the X-radiation, the reflectivities from both kind of domains must be superimposed (incoherent superposition). At very small or very high covering efficiencies ($c < 0.05$ or $c > 0.95$), both procedures give similar results, but at $0.05 < c < 0.95$ the results are significantly different. In this study the agreement between the measured data and the corresponding fits at intermediate covering efficiencies was only achieved in the framework of the incoherent superposition approximation. The reflectivity of a pure monolayer ($R_{mono}(q_z)$) was thus combined with the reflectivity of a monolayer with a bound protein layer ($R_b(q_z)$):

$$R_{tot}(q_z,t) = [1 - c(t)] \cdot R_{mono}(q_z) + c(t) \cdot R_b(q_z,t) \quad (4)$$

$c(t)$ being the extent of the covered surface and t the time after the addition of proteins. The fact that only Eq. (4) describes the observed reflectivity curves in their integrity suggests that the size of the covered and uncovered surface regions in our experiments was of the order of μm, in the range of $0.05 < c < 0.95$, at least.

Surface covering by the binding protein thus starts as dense 'islands' that grow in size, but not in thickness, with the progressive covering of the investigated surface area. The bare and the covered surface layer regions, consequently, are describable within the framework of a time-dependent, Gaussian-smeared two- or three-box model, respectively.

2.3.4. Protein binding kinetic

In principle protein binding onto a monolayer is a two-step process. The first step is the diffusion of proteins from the bulk to the monolayer. The second step is the binding of proteins onto the specific binding sites located in the free surface area of the monolayer. The predominance of one step or the other depends on the diffusion coefficient D, on the surface concentration of protein and on the accessibility of the specific binding sites. Typical diffusion coefficients for the proteins such as concanavalin A are of the order $(10^{-10}–10^{-11})$ m^2 s^{-1}, [1]. The mean square distance travelled by the diffusing proteins, $\bar{x}^2$, is given by the relation: $\bar{x}^2 = 2Dt \sim 10$ μm $\cdot \sqrt{t/s}$ [1]. Due to the thin sample (~ 300 μm) the bulk protein concentration variabilities therefore disappear within minutes which is faster than the measured characteristic times of protein binding. The distribution of proteins in the bulk may thus be assumed to be constant, so that the binding kinetic of concanavalin A depends on the bulk protein concentration rather than being under diffusion control [10].

The number of proteins binding to and desorbing from the receptor-containing interface, $dn_p(t)$, in the simplest approximation, is given by

$$dn_p(t) = k_a \varrho_p A(t) dt - (A - A(t)) k_d dt \quad (5)$$

$$= \frac{1}{6} \varrho_p A(t) v_p dt - (A - A(t)) k_d dt \quad (6)$$

k_a and k_d are the adsorption (binding) and desorption constants. $A(t) = A\text{-}n_p(t) \cdot A_p$ is the uncovered surface region and ϱ_p is the volume density of proteins. A and A_p are the total surface area and the protein cross-section area, respectively. v_p is the protein diffusion velocity. The factor $\frac{1}{6}$ allows for the different directions of motion. The dependence of the rate of binding on random collisions does not necessarily imply that the lectin distribution on the surface is also random. Eq. (6) is not affected by the lateral aggregation of the adsorbed material as long as the interaction between the open area and the adsorbent is unchanged. For the specific short range interactions, such as lectin-sugar binding, this should be the case.

Solving Eq. (6) and rewriting the result in terms of the surface covering efficiency gives:

$$c(t) \overset{def}{=} \frac{A - A(t)}{A}$$

$$= \frac{K\varrho_p}{1 + K\varrho_p} \cdot \left\{1 - \exp\left[-\left(k_a \varrho_p + k_d\right)t\right]\right\} \quad (7)$$

$$= \frac{K\varrho_p}{1 + K\varrho_p} \cdot \left\langle 1 - \exp\left[-\left(\frac{1}{6}\varrho_p A_p v_p + k_d\right)t\right]\right\rangle \quad (8)$$

$K = (k_a)/(k_d)$ is the equilibrium constant of protein adsorption and desorption. The concentration dependent prefactor describes a 'Langmuir-isotherm'.

The measured mono-exponential time dependence of the surface coverage must be compared with the time factor calculated from Eq. (8), where the theoretical diffusion velocity, $v_p = D/l$, is given by the Einstein-Smoluchowski equation:

$$v = \frac{k_B T}{2\pi\eta r l} \approx 1.6 \cdot 10^{-4} \mathrm{ms}^{-1} \quad (9)$$

in which k_B is the Boltzmann constant, T the temperature, η the viscosity ($= 1.00103 \cdot 10^{-3}$ Pa s for water at 20°C), r the radius of the diffusing particle (~ 4 nm, [2]) and $l \approx \sqrt[3]{\varrho_p^{-1}}$ the free-path length.

3. Results

3.1. Binding to the surface

DSPE-mal$_1$ and its interaction with concanavalin A was studied on the reflectometer described by Metzger et al. [12].

After an equilibration time of 5 h, the mixed phospholipid-monolayer (DSPC:DSPE-mal$_1$ 20:1 mole:mole) at the air-suspension interface was found to be stable and gave the reflectivity shown in Fig. 2a as a function of the vertical wave vector transfer, q_z, given in units of the critical wave vector transfer of total reflection of a pure water surface, $q_c = 0.02179$ Å^{-1}. (In order to emphasize the interesting features

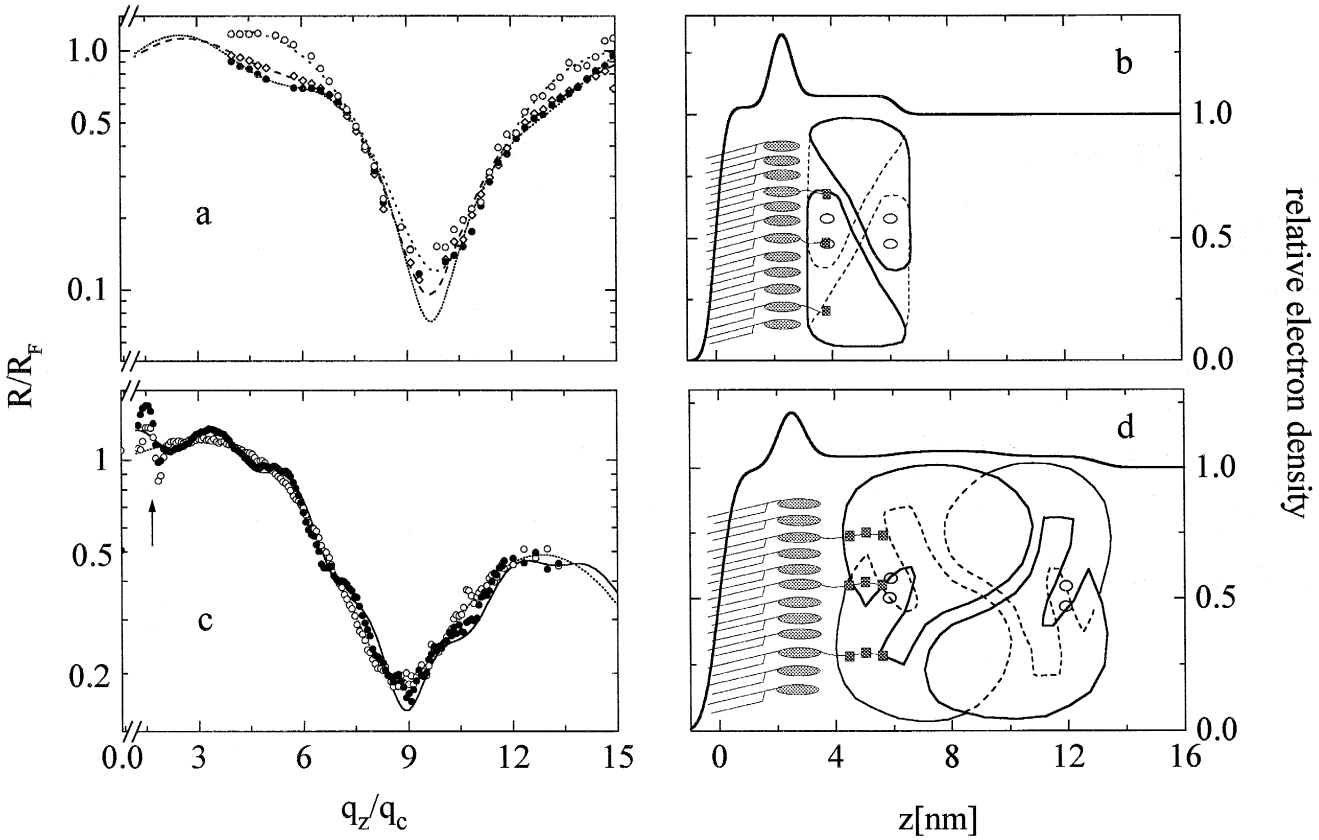

Fig. 2. The measured reflectivity (symbols) normalized with regard to the Fresnel-reflectivity of an ideally smooth water surface and data fits (lines) done in the framework of a Gaussian-smeared three-box model. DSPC/DSPE-mal$_1$ (20:1 mol:mol), $c_{Con\ A} = 0.1$ mg/ml, ○ $t < 0$, ◇ $t = 20$ h, ● $t = 30$ h (upper left panel), relative electron density profile at t = 30 h (upper right panel) and DSPC/DSPE-mal$_3$ (10:1 w:w), $c_{Con\ A} = 0.1$ mg/ml, ○ $t < 0$, ● $t = 300$ min (lower left panel), relative electron density profile at $t = 300$ min (lower right panel). The electron density profiles are clarified by the cartoons drawn to the scale. (Small, open circles indicate the positions of specific binding sites for sugar.) The arrow indicates the region of imperfect calibration due to the characteristic tungsten L-lines.

Table 1
Structural parameters of various phospholipid monolayers with or without adsorbed concanavalin A layer at the air–water interface

	ρ_c	ρ_h	ρ_b	d_c [nm]	d_h [nm]	d_{ads} [nm]	θ [°] †	A_l [nm^2] ‡	σ [nm] ♯	Ref.
Concanavalin A tetramer	–	–	–	–	–	$\sim 3.9\times 8.0\times 9.0$	–	–	–	[2]
DSPC/DSPE-mal$_1$ *	1.03 ± 0.03	1.41 ± 0.04	1.08 ± 0.02	1.93 ± 0.08	0.68 ± 0.06	3.63 ± 0.18	27 ± 5	0.445 ± 0.015	0.29 ± 0.02	this work
DSPC/DSPE-mal$_3$ **	0.99 ± 0.02	1.40 ± 0.03	1.06 ± 0.02	2.17 ± 0.08	0.66 ± 0.07	9.7 ± 0.5	13 ± 8	0.439 ± 0.015	0.43 ± 0.03	this work
DSPC ***	1.01 ± 0.04	1.43 ± 0.05		1.92 ± 0.08	0.73 ± 0.06		27 ± 6	0.439 ± 0.015	0.44 ± 0.03	this work
DSPC ****	0.90 ± 0.01	1.44 ± 0.04		1.97 ± 0.05	0.74 ± 0.05		30 ± 3	0.460 ± 0.005		(calculated) *
DPPC	0.90 ± 0.01	1.44 ± 0.04		1.75 ± 0.05	0.74 ± 0.05		30 ± 3	0.460 ± 0.005		[17]
DPPC	0.919 ± 0.009	1.34 ± 0.04		1.60 ± 0.06	0.93 ± 0.04		33 ± 3	0.447 ± 0.006	0.42 ± 0.02	[15]

† Calculated on the basis of Eq. (10).
‡ Calculated on the basis of Eq. (11).
♯ This value depends on the sample thickness and resolution. Theoretical value is 1.8 Å, [4].
* DSPC/DSPE-mal$_1$.
** DSPC/DSPE-mal$_3$.
*** DSPC monolayer in contact with a DSPC vesicle suspension (10 mg/ml, sonicated, diameter $\sim$150, data not shown).
**** d_c data were obtained by interpolation from the DPPC data from [17] using $d_{c,DSPC} = d_{c,DPPC} + 2\cdot\cos(\theta)\cdot 1.265$ Å; all other values are identical with those pertaining to DPPC.

in this and all other reflectivity curves shown, the data-sets were normalized with regard to the calculated Fresnel-reflectivity of an ideally smooth water surface.) Comparison of calculated and measured reflectivity curves yielded a set of optimal model parameters given in Table 1.

When a solution of maltose- or glucose-recognizing lectin, concanavalin A, is injected at $t = 0$ under the equilibrated DSPC monolayer, doped with the appropriate receptor glyco-lipid, DSPE-mal$_1$, the reflectivity curve begins to change characteristically (Fig. 2a). Most obviously, the reflectivity (recorded every 2.5 h) decreases close to $5q_c$, $10q_c$, and $15q_c$. The reason for this is the destructive interference of the radiation scattered at the head-group/lectin and lectin/water interfaces.

To simulate the temporal variability of the interfacial structure caused by protein binding in a first fitting round all model parameters (the relative electron densities of lipid monolayers with and without adsorbed lectin (ρ_c, $\rho_{c,ad}$, ρ_h, $\rho_{h,ad}$), the adsorbed layer density (ρ_b), but also the corresponding layer thicknesses (d_1, $d_{1,ad}$, d_2, $d_{2,ad}$, d_3), the global surface smearing parameter (σ), and the covering efficiency parameter (c)) are fitted simultaneously to the measured reflectivity data. Starting model parameters inserted into the least χ-square fit algorithm were chosen consistent with the literature. Minimizing χ-square gives the reflectivity curves shown in Fig. 2a. The final covering efficiency is close to 1. No significant or systematic variations are recognizable within the experimental error in the calculated, layer-characterizing structural parameters at any time. Results for the adsorbed protein layer are shown in Fig. 3a,b.

The lipid monolayer at the air–water interface is little affected by the binding of concanavalin A. It is hence permissible to assume that all monolayer-describing parameters are constant and identical to the values found for $c = 0$ (where the data-fits are most sensitive to the monolayer-parameters). This minimizes the statistical error associated with the determination of covering efficiency from the measured reflectivity data. The model parameters describing the protein layer also may be set equal to the corresponding values pertaining to $c = 1$.

The corresponding values are given in Table 1. The appropriate electron density profile is shown in

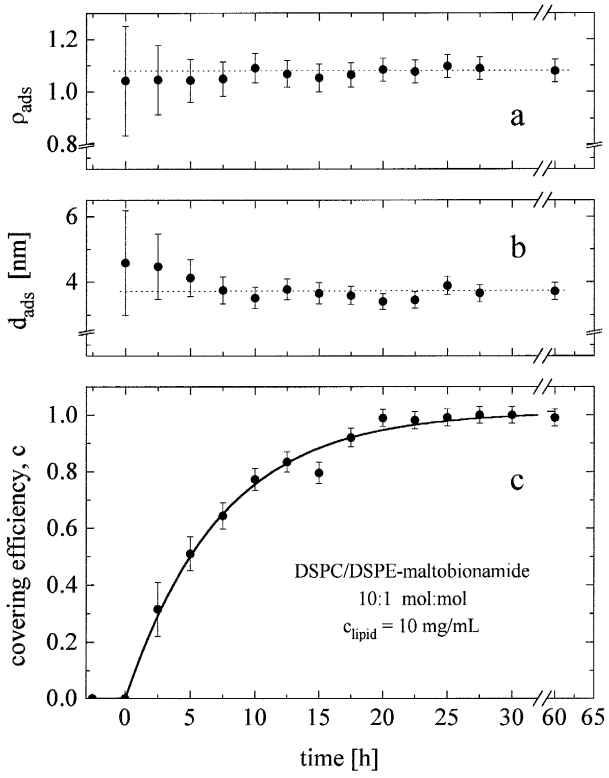

Fig. 3. Top: Temporal development of the model parameters describing the concanavalin A bound onto a DSPC/DSPE-mal$_1$ monolayer (20:1 mole:mole) in the framework of a Gaussian-smeared three-box model. $c_{Con\ A} = 0.1$ mg/ml. Bottom: Temporal development of the corresponding covering efficiency.

Fig. 2b. The corresponding time-dependence of protein binding is described well by the mono-exponential curve with the characteristic time of $\tau_p = (7.0 \pm 0.3)$ h and amplitude $c = 1$ (Fig. 3c).

DSPE-mal$_3$ and its interactions with the concanavalin A molecules were characterized with the improved reflectometer (Fig. 1) which ensured better time- and space-resolution. The DSPC/DSPE-mal$_3$ monolayer (10:1 w:w) was prepared as described in the previous section and placed over a 0.3 mg/ml suspension of the corresponding lipid vesicles in a 10 mM K-phosphate buffer pH 7 containing 2 mM EDTA. The bulk concentration of concanavalin A was then chosen to be between 0.01 mg/ml and 0.10 mg/ml. Representative, normalized reflectivity curves measured for 15 min are shown in Fig. 2c for $c_{con\ A} = 0.1$ mg/ml before and 300 min after addition of protein. This reveals the characteristic reflectivity changes in certain q_z-regions, most notably

near $5q_c$, $7q_c$ and $9q_c$. At these points in q-space the reflectivity gradually decreases with time due to the destructive interference of the radiation scattered at the headgroup/lectin and lectin/water interfaces.

The data measured with DSPE-mal$_3$ monolayers were evaluated as described before. Now, the excellent data quality allowed the variation of all parameters. As in the case of DSPE-mal$_1$-layers, no significant change was detected in the structural parameters during the protein binding (Fig. 4a,b, mean values are given in Table 1). The differences between the different results are within the experimental error. The lower reflectivity at high q_z/q_c in comparison with the DSPE-mal$_1$ reflectivity is due to the higher interfacial roughness (see Eq. (3) and discussion).

The time dependence of binding to the surface as a function of the bulk protein concentration is shown in Fig. 4c. Comparison of Figs. 3 and 4 reveals that while the binding kinetic of concanavalin A to the DSPC/DSPE-mal$_1$ and DSPC/DSPE-mal$_3$ is very different, the kinetic at different protein concentrations is quite similar, ~ 1 h (see Fig. 5c). This finding will be discussed further in the following section.

The final covering efficiency for DSPE-mal$_3$ decreases with decreasing bulk protein concentration. Fitting the values with a Langmuir-isotherm according to Eq. (8) (where ϱ_p is the nominal concentration of the concanavalin A tetramers) reveals a nominal equilibrium constant $K \sim (1.6 \pm 0.7) \cdot 10^{-20}$ m^3 = $(9.6 \pm 4.2) \cdot 10^6$ M^{-1}. As we will see in the following section, this value must be corrected for the lower, effective protein concentration by a factor of ~ 10–1000.

3.2. Binding in the bulk

Based on Eq. (9), and the specific experimental conditions of our investigations, one would expect the characteristic time-constant of protein binding to be of the order of seconds. In reality, however, this process can be fitted with a single exponential curve with the time constant of the order of hours (Fig. 3c and Fig. 4c).

This conflict can be resolved easily by assuming that the bulk protein concentration decreases rapidly by several orders of magnitude owing to the protein adsorption on the vesicles in the bulk. This leaves only a small, constant protein amount in the solution already a few minutes after the protein addition. At later times, the quasi-stationary state is hence established in which the protein binding to and desorption from the vesicle surface are nearly balanced. As argued before protein bulk concentration is then constant, but has a value much smaller than the nominal, starting protein bulk concentration.

We have tried to check this postulate by inserting the diffusion velocity into the nonlinear differential equation describing the bulk protein concentration as a function of time (not shown) in the presence of

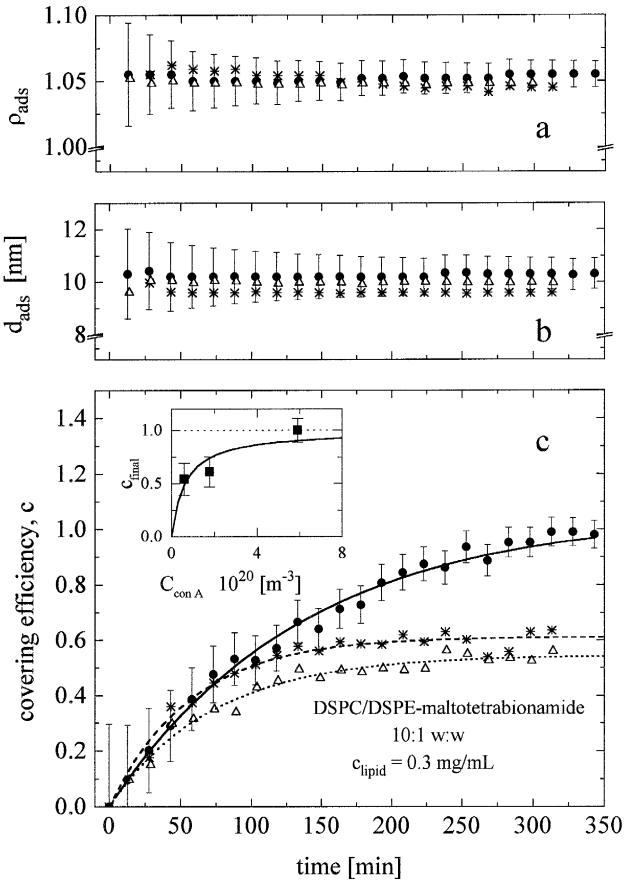

Fig. 4. Top: Temporal development of the model parameters describing the protein layer adsorbed onto a DSPC/DSPE-mal$_3$ monolayer (10:1 w:w) in the framework of a Gaussian-smeared three-box model. ● $c_{Con\ A} = 0.10$ mg/ml, * $c_{Con\ A} = 0.03$ mg/ml, △ $c_{Con\ A} = 0.01$ mg/ml. Bottom: Temporal development of the corresponding covering efficiency. Representative error bars are shown only for $c_{Con\ A} = 0.10$ mg/ml. Inset: concentration dependence of the final surface covering efficiency (■) and the corresponding Langmuir-isotherm (see Eq. (8)).

uniformly distributed protein-binding sites (vesicles). Numerical integration showed that, indeed, the bulk concentration drops from 10^{-1} mg/ml to a much lower, but constant, value within less than one minute. Specific binding of small proteins, such as concanavalin A, is known to be a very fast process. This suggests that typical protein binding time, under our experimental conditions, is not governed by the speed of protein-binding as such; rather than this, it is controlled by the rate of collision between the binding molecules and the monolayer-solution interface. Due to the vast disproportion between the lipid monolayer surface and the total surface of lipid vesicles in the bulk the latter deplete proteins rapidly in the bulk. This lowers the probability for the proteins impact at the interface – and therefore slows down the kinetics of protein binding onto the monolayer dramatically.

In order to verify the above assumption experimentally, we measured the turbidity of the suspensions of sonicated vesicles (diameter ~ 70 nm) keeping the composition and the bulk lipid concentration the same as in our reflectivity measurements. This was done under constant temperature and with stirring. Due to the existence of multiple binding sites for the concanavalin A tetramers, protein binding entailed vesicle aggregation which increased the sample turbidity (see Fig. 5a,b). At low lectin concentrations, the addition of Concanavalin A induced a step-like jump in the sample turbidity which was followed by the slow mono-exponential increase. This observation is evident at low protein concentrations (Fig. 5b) but probably also holds at the higher concentrations where no satisfactory data fits were possible with a single mono-exponential curve.

This supports the suggested two-step binding model: immediately after the addition of concanavalin A the proteins begin to adsorb locally to the vesicles in the bulk. This lowers the effective bulk protein concentration c_{eff} and is followed by a slow equilibration process that leads to the homogeneous covering of the entire lipid interface, including the vesicles as well as the monolayer surface. The kinetics of the slow equilibration process is governed by the effective protein concentration in the bulk. Increasing the initial protein concentration thus results in the faster kinetics.

By taking this two-step model into account all curves were fitted by superimposing two mono-exponential curves with different exponential time factors $\tau_1 \sim$ s and $\tau_2 \sim$ min…h. The results of such model calculation are given in Fig. 5c together with the data stemming from the reflectivity measurements. The rate of protein binding to the vesicles and

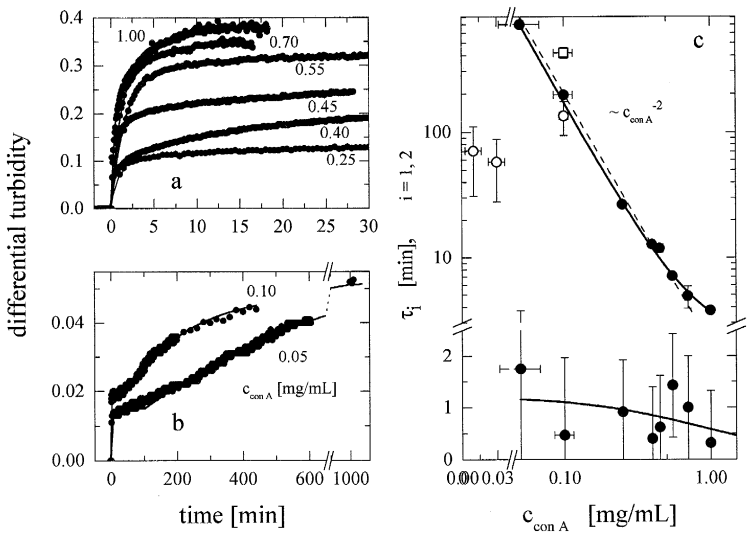

Fig. 5. Temporal dependence of the differential turbidity of a sonicated vesicle suspension with identical composition as in the corresponding reflectivity measurements at different initial protein concentrations (left). The measured data were fitted with a superposition of two mono-exponential curves (see the text). Results are given on the right side. Lower set τ_1, upper set τ_2. Results of reflectivity measurements are shown as open symbols (○ DSPE-mal$_3$, □ DSPE-mal$_1$).

to the monolayer needs not to be identical, but should have similar time constants. Therefore, in Fig. 5c time constants for the binding to the monolayer are shown for purpose of comparison.

The initial step in the protein binding is described by Eq. (8) with ϱ_p being the total concentration of concanavalin A tetramers. τ_1 therefore corresponds to the inverse prefactor in the exponential argument, $\tau_1 = (k_d(K\varrho_p + 1))^{-1}$. This exponential time-factor is resolved poorly in our experiments, as it is short, ≤ 1 min. Fitting the relation between τ_1 and k_d, K and ϱ_p to the measured values (Fig. 5c) gives estimates for $K \approx (1.9 \pm 2.6) \cdot 10^{-19}$ m^3 $= (1.1 \pm 1.6) \cdot 10^8$ M^{-1} and for $k_d \approx (0.014 \pm 0.005)$ s^{-1}. In the first approximation one may assume that the equilibrium constants derived from the bulk- and the surface measurements are identical. The effective protein concentration, decisive for the slow equilibration process and the binding on the monolayer, is then by a factor of 10–1000 lower as mentioned before. The desorption rate, k_d, is very low, however, as expected for the specific binding.

Interestingly, τ_2, as measured in the turbidity measurements, seems to be inversely proportional to the square of initial protein concentration (at least for $c_{con\ A} < 0.7$ mg/ml).

3.3. Structural parameters

The hydrocarbon tilt in the surface-adsorbed lipid monolayer is given by:

$$\theta = \arccos \frac{d_c}{l_c} \tag{10}$$

$l_c = (n_c\text{-}7/8) \cdot 0.1265$ nm being the length of the fully extended acyl chains with n_c carbon atoms [11]. Using Eq. (10) together with the data from Table 1, one gets $\theta = (27 \pm 5)°$ for DSPC/DSPE-mal$_1$ and $\theta = (13 \pm 7)°$ for DSPC/DSPE-mal$_3$. The published tilt of DSPC is $30 \pm 3°$ [17]. The low tilt-angle value determined for the DSPC/DSPE-mal$_3$ mixed-lipid layers could be due to the presence of sugar-lipids, which introduce regions of low electron density in the headgroup region and thus shift the border between the chain- and headgroup region to an apparently greater z-value; the narrow 'headgroup-box' is indicative of this. The partial lipid headgroup dehydration at the air–water interface could also diminish the hydrocarbon tilt angle value [6].

The cross-section of each lipid molecule (perpendicular to the lipid chains) can be estimated from the phenomenologic expression:

$$A_l = \frac{Z}{(d_c \rho_c + d_h \rho_h)\rho_{water}} \tag{11}$$

in which Z gives the total number of electrons in each lipid molecule (for DSPC: $= 438$) and $\rho_{water} = 334$ e $\cdot$ nm^{-3} is the electron density of water. Eq. (11) gives the value of $A_l = 0.445 \pm 0.015$ nm^2 for DSPC/DSPE-mal$_1$ and $A_l = 0.439 \pm 0.015$ nm^2 for DSPC/DSPE-mal$_3$. The generally accepted value for the tightly packed pure phosphatidylcholine is 0.42 ± 0.02 nm^2, [5].

The results for bound protein and lipid layers are given in Table 1. For comparison the results of independent measurements with a pure DSPC monolayer and with the DPPC monolayer are also presented. For experimental details see footnote to Table 1.

4. Discussion

4.1. X-ray reflectivity measurements

Phosphatidylcholine packing in the pure DSPC or in the mixed DSPC/sugar-lipid monolayer appears to be similar. This indicates that glycolipids do not disturb the structure of DSPC layers appreciably, at least when they are added in small amounts.

The electron density in the headgroup region, the thickness of headgroup- and chain-regions, as well as the calculated chain tilt, within the experimental error, agree with the results of previous studies (notice the differences in chain-lengths, however!). Exceptional are solely the DSPE-mal$_3$ layers (see previous paragraph) and, perhaps, the electron density in the hydrocarbon region. The latter significantly exceeds the previous estimates based on the results of X-ray reflectivity measurements. This, on the one hand, could be due to the ambiguity of box-models that are commonly used in the evaluation of X-ray reflectivities: For example, if some electrons in the glycerol

backbone region in the one case are assigned to the headgroup and in the other situation are assumed to belong to the chains, the two sets of results will differ considerably. Such an interference is supported by the good consistency of lateral packing parameter A_l calculated from Eq. (11) and from the measured X-ray reflectivity data: being an integral quantity of the system the area per lipid molecule is not affected by such model ambiguity.

The differences between various surface roughness parameters as documented in Table 1 are insignificant. The measured interfacial roughness is not identical to the intrinsic, microscopic interfacial roughness. This quantity includes the contributions from the thermically stimulated capillary waves which scale with the water layer thickness and temperature and from the limited reflectometer resolution [4]. Both contributions increase the apparent measured roughness and differ widely between the laboratories owing to the different experimental and instrumental conditions. Theoretical value for the capillary wave contribution of the pure water surface, derived from a capillary wave model, is 0.18 nm [4].

Significant differences exist, however, between the results of X-ray small angle scattering experiments and data obtained from the combined X-ray and neutron reflectivity measurements [17]. This discrepancy is not surprising in light of the different physical basis of these two types of experiments: X-ray reflectivity measures the surface electron density profiles; neutron reflectivity, conversely, senses the contrast in neutron scattering-length density profiles. Consequently, one also should not expect *nominally* similar box-model parameters *actually* to have identical values.

In our model the interfacial roughness is set to be equal for all interfaces in order to reduce the number of adjustable parameters in the fits. The water/protein-layer interface is definitely more rough than the monolayer interfaces, however, at least in the case of incomplete covering. The values given in Table 1, therefore, overestimate the roughness of the monolayer interfaces and underestimate the roughness of the water/protein-layer interface. The introduction of the protein-layer roughness as an additional parameter would damp the oscillations in the reflectivity due to the interference between the reflection on the lipid/lectin- and lectin/water-interface. This would give a better match of the fits at high q_z/q_c-values but was not attempted here, in order to minimize the statistical variations (see below).

Last but not least, it is desirable to estimate the maximum spatial- and time-resolution of the experimental data presented in this work. To this end we have simulated the hypothetical reflectivity curves with the electron density profiles pertaining to the slightly altered or structured layers. This was done by altering the box parameters or adding new boxes. (The latter is believed to represent, in the first approximation, the fine structure of the surface-adsorbed concanavalin A layer.) Protein layer was normally separated into three boxes centered in the middle of the bound protein layer. This was motivated by the tetrameric structure of concanavalin A molecules as well as by the intrinsic symmetry of this protein with regard to its midplane (see cartoon in the electron density profiles in Fig. 2, [2]). For DSPE-mal$_3$ the midplane was also shifted by the calculated length of the tetrabionamide group in order to check whether the sugar group shifts the center of symmetry away from the lipid–protein interface. For all other simulations the midplane was taken to coincide with the center of the bound protein layer. These simulations (not shown) gave the experimental errors listed in Table 1.

The experimental error associated with monolayer parameters is smaller than that of the protein layer. This is largely due to the higher electron density contrast between the chain- and headgroup regions that increase the effective differences in the reflectivity curve (see Eq. (2)). For the structured model-profiles only the one with a flat maximum in the middle of each concanavalin A molecule (amplitude $\sim 10\%$ of the contrast) provided a better fit. The difference was not statistically significant, however. This could be a mirror of the overall ellipsoidal shape of concanavalin A tetramers [2]. Shifting the plane of symmetry away from the protein–lipid interface results in a large deviation from the measured reflectivity at all local minima. The inner structure of protein layer therefore seems to be symmetric around the center of the bound protein layer.

The introduction of more degrees of freedom into the data fits, that is, the use of more adjustable parameters (boxes, roughnesses) would introduce the fitting of statistical changes in the recorded reflectiv-

ity curves. This would produce unrealistic changes in the calculated electron density profiles. In light of the inevitably large statistical errors in our time-resolved data, we have thus chosen to stick to the three-box model with one global interfacial roughness parameter, to minimize the statistical variations.

Further improvement of the spatial resolution could be achieved by prolonging the recording times. This would decrease the statistical error but also the time resolution. Alternatively the observed wave-vector region could be increased. The former option is always feasible but the latter may be precluded by the smearing of reflectograms in the range of large q_z-values, which results from the surface-roughness effects. Another solution to this problem is to improve the contrast by the introduction of heavy-atoms into the studied layers or into the substrate.

We are currently working on this latter extension of X-ray reflectivity measurements. In the present work, its potential advantage is reflected in the fact that the lipid monolayer structure is modeled with a much better accuracy (≤ 0.1 nm) than the bound proteins (< 0.5 nm), owing to the better electron density contrast between the lipid chain- and headgroup regions.

A striking feature in our data pertaining to the different concanavalin A-binding molecules (DSPE-mal$_1$ and DSPE-mal$_3$) is the discrepancy between the measured thickness of the adsorbed protein layer, which is 3.9 nm and 9.7 nm for the glycolipids with 1 and 3 sugar residues, respectively. These values must be compared with the protein dimensions. Concanavalin A protomers are known to be ellipsoidal domes with dimensions of $(4.2 \times 4.0 \times 3.9)$ nm^3 and molecular weight 25.5 kDa [2]. In an aqueous solution such protomers aggregate spontaneously into the flat tetramers with an estimated area of 72 nm^2, about 160 times larger than the area of each phosphatidylcholine molecule (Table 1). Tetramers measure $\sim (3.9 \times 8.0 \times 9.0)$ nm^3. The protein layer thickness near the DSPE-mal$_1$-layer therefore agrees well with the thickness of a flat concanavalin A tetramer (~ 3.9 nm [2]). Conversely, the protein layer thickness near the DSPE-mal$_3$ layer comes very close to the greatest length of a concanavalin A tetramer (~ 9 nm) or to the sum of the smaller side and the length of 3 sugar-residues and the spacer ($\sim 8 + 1.7$ nm). (The dimensions of the glycolipid head-group were determined from computer simulations.) The fact that the specific binding sites for sugar on concanavalin A are located ca. 1.5 nm from the long side of such protein tetramer, but more than 4 nm from the short side (from [2], see cartoons in Fig. 2), suggests that the lectin molecules adsorb flat on the DSPC/DSPE-mal$_1$ monolayer. In the vicinity of a DSPC/DSPE-mal$_3$ monolayer the concanavalin A molecules seem to bind 'on the side' and to point from the surface with their long side. The length of sugar residue DSPE-mal$_3$ is compatible with binding to two different orientations, but only one is found. This suggests that this latter conformation is energetically favoured.

4.2. Bulk measurements

The τ_2-values measured in our reflectivity experiments with the identical DSPE-mal$_3$ samples agree with the values deduced from the turbidity measurements when $c_{con\ A} = 0.10$ mg/ml (Fig. 5c). However, the values pertaining to $c_{con\ A} = 0.01$ mg/ml and $c_{con\ A} = 0.03$ mg/ml are significantly smaller near the surface. Two explanations can be given for this: the first is the limited temporal resolution of the reflectivity data which precludes unequivocal fits with two mono-exponential curves. (A potentially not-resolved step in the covering efficiency at the beginning of an experiment would result in an underestimate of the value of τ_2.) Secondly, there is no reason why the details of protein binding to the monolayer and to the vesicle surface should be the same; the different time constants could be indicative of the unequal interaction potentials between the protein and vesicle and protein and monolayer.

The rate of concanavalin A binding to the DSPE-mal$_1$ monolayer for $c_{con\ A} = 0.10$ mg/ml (open square in Fig. 5) is lower than in the case of the DSPE-mal$_3$ membrane. The reflectivity as well as the turbidity measurement both suggest this. Such a discrepancy can be explained by the poorer accessibility of binding sites on concanavalin A for the shorter sugar residues of DSPE-mal$_1$ in comparison with the DSPE-mal$_3$, which has 3 rather than 1 hexoses in its headgroup. The more effective reduction of protein concentration difference due to the higher lipid concentration $(30\times)$ could also be important.

Finally, one would like to know the driving force for the progressive protein binding to the lipid mono-

layer. What drives the protein to the surface after most of the proteins have already bound to the vesicles in the early, rapid stage of glycolipid-concanavalin A association? There are several answers to this question. The repulsion between the lipid monolayer and proteins is probably weaker than between the lipid vesicles and the lectins in the bulk. The partial lipid dehydration at the air–water interface may be the reason for this as well [7]. The Van der Waals-attraction at the air–water interface is also higher than in the bulk, due to the lower dielectric constant of the background [8]. The re-distribution of protein between the vesicles and the surface could also play some role [1], being one possible reason for the higher cooperativity of protein binding to the perfectly flat surface layer. The importance of this latter phenomenon remains to be shown by means of the grazing-incidence X-ray reflectivity (GID), for example, which to date can only be done with synchrotron light. We believe that the more convenient binding-layer geometry as well as the stronger Van der Waals attraction of the monolayer are dominant in this respect.

In summary, we have shown that the energy-dispersive reflectivity measurements are a powerful tool for investigating the interfacial (re)structuring near the air–water boundary. This pertains to the time-scale of less than one hour and to the spatial resolution between 0.1 nm and 0.5 nm when a laboratory based, low-intensity X-ray reflectometer is used. Such an instrument can therefore be used to study the structural rearrangement near different surfaces. Our study of the slow binding of lectin to the (glyco)lipid monolayer at the air–water interface provides an illustrative example for this. The time-dependent surface-induced phase changes or the surface-dependent phase transitions could be monitored next. In combination with the high intensity synchrotron radiation measurements on the time-scale of < 1 minute should be possible.

[1] In this context it is important to remember that the total surface of vesicles exceeds by several orders of magnitude the surface of the lipid monolayer. Therefore, the covering efficiency of lipid vesicles is not affected by the amount of proteins adsorbed to the monolayer.

Acknowledgements

This study was supported by the Bundesministerium für Forschung und Technologie through Grants 5 WOM X2 (Cevc B). We thank Dr. Hartmut Metzger of the Ludwig Maximilians-Universität München for the use of his X-ray facility in the early phase of this study and for the stimulating discussions.

References

[1] Atkins, P.W. (1990) Physical Chemistry, 4th edition. Oxford University Press.
[2] Becker, J.W., Reeke Jr., G.N. Wang, J.L., Cunningham, B.A. and Edelmann, G.M. (1975) J. Biol. Chem. 250, 1513–1424.
[3] Blume, G. (1991) Liposomen für den systemischen Einsatz in der Medizin, Ph.D. Thesis, TU München.
[4] Braslau, A., Pershan, P.S., Swislow, G., Ocko, B.M. and Als-Nielsen, J. (1988) Phys. Rev. A 38, 2457–2470.
[5] Cevc, G. (ed.) (1993) Phospholipids Handbook. Marcel Dekker.
[6] Cevc, G. (1991) Biochim. Biophys. Acta 1062, 59–69.
[7] Cevc, G., Fenzl, W. and Sigl, L. (1990) Science 249, 1161–1163.
[8] Cevc, G. and Marsh, D. (1987) Phospholipid Bilayers. Physical Principles and Models. Wiley, New York.
[9] Dalliant, J., Benattar, J.J. and Leger, L. (1990) Phys. Rev. A, 41, 1963–1977.
[10] Eddowes, M.J. (1986) Biosensors 3, 1–15.
[11] Helm, C.A., Tippmann-Krayer, P., Möhwald, H., Als-Nielsen, J. and Kjaer, K. (1991) Biophys. J. 60, 1457–1476.
[12] Metzger, T.H., Luidl, C., Pietsch U. and Vierl, U. (1994) Nuclear Instruments and Methods in Physics Research A, 350, 398–405.
[13] Russell, T.P. (1990) Materials Sci. Rep. 5, 171–271.
[14] Salditt, T., Rhan, H., Metzger, T.H., Peisl, J., Schuster, R. and Kotthaus, J.P. (1994) Z. Phys. B 96, 227–230.
[15] Vaknin, D., Kjaer, K., Als-Nielsen, J. and Lösche, M. (1991) Biophys. J. 59, 1325–1332.
[16] Vierl, U., Cevc, G. and Metzger, H. (1995) Biochim. Biophys. Acta 1234, 139–143.
[17] Wiener, M.C., Suter, R.M. and Nagle, J.F. (1989) Biophys. J. 55, 315–325.
[18] Williams, T.J., Plessas, N.R., Goldstein, I.J. and Loengren, J. (1979) Arch. Biochem. Biophys. 195, 145–151.